The Geometry of 2D Image Signals*

Lennart Wietzke , Gerald Sommer and Oliver Fleischmann
Cognitive Systems Group
Kiel University, Department of Computer Science
Christian-Albrechts-Platz 4, D-24118 Kiel, Germany
lw@ks.informatik.uni-kiel.de

Abstract

This paper covers a fundamental problem of local phase based signal processing: the isotropic generalization of the classical 1D analytic signal to two dimensions. The well known analytic signal enables the analysis of local phase and amplitude information of 1D signals. Local phase, amplitude and additional orientation information can be extracted by the 2D monogenic signal with the restriction to the subclass of intrinsically one dimensional signals. In case of 2D image signals the monogenic signal enables the rotationally invariant analysis of lines and edges. In this work we present the 2D analytic signal as a novel generalization of both the analytic signal and the 2D monogenic signal. In case of 2D image signals the 2D analytic signal enables the isotropic analysis of lines, edges, corners and junctions in one unified framework. Furthermore, we show that 2D signals exist per se in a 3D projective subspace of the homogeneous conformal space which delivers a descriptive geometric interpretation of signals providing new insights on the relation of geometry and 2D signals.

1. Introduction

Low level two-dimensional image analysis is often the first step of many computer vision tasks. Therefore, local signal features with geometrical and structural information determine the quality of subsequent higher level processing steps. It is important not to lose or to merge any of the original signal information within the local neighborhood of the test point. The constraints of local signal analysis are: to span an orthogonal feature space (split of identity) and to be robust against stochastic and deterministic deviations between the actual signal and the assumed signal model. One of the fundamental problems in signal processing is a good signal representation. Such a signal representation is the local phase information which is a robust feature with respect to noise and illumination changes [10, 7, 6]. In case of image signals it is shown in [12] that the original signal can be recovered to a fairly large extend by using only its phase information while setting its amplitude information to unity. In contrast to that, if only the amplitudes are obtained and the phases are set to zero, the recovered image signal is completely indiscernible. Therefore, phase based signal processing has found success in many applications, such as disparity estimation of stereo [7], matching [2], face recognition [17], optical flow estimation [18], etc.

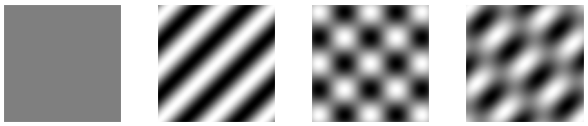

Figure 1. From left to right: i0D signal, i1D signal with $n = 1$ in Equation (1) to model straight lines and edges in scale space and two i2D signals which consist of two superimposed i1D signals with $n = 2$ in Equation (1) to model locally junctions and corners in scale space.

2. Local pattern modeling

Based on the results of Fourier theory and functional analysis we assume that each 2D signal $f \in L^2(\mathbb{R}^2) \cap L^1(\mathbb{R}^2)$ can be locally modeled by a superposition of arbitrarily orientated one-dimensional cosine waves [16]

$$\mathcal{P}\{f\}(z;s) = (p * f)(z;s) = a_s \sum_{\nu=1}^{n} \cos(\langle z, \bar{o}_{s,\nu} \rangle + \phi_s) \quad (1)$$

with $z = (x, y)$, $*$ as the convolution operator and $\bar{o}_{s,\nu} = [\cos\theta_{s,\nu}, \sin\theta_{s,\nu}]^T$. The Poisson convolution kernel [5] reads

$$p(z;s) = \frac{s}{2\pi \left(s^2 + \|z\|^2\right)^{3/2}} \quad (2)$$

(see Figure 2) for a certain scale space parameter $s \in \mathbb{R}_+$ which acts as a low pass filter on the original signal f. Without loss of generality this signal model degrades locally at

*We acknowledge funding by the German Research Foundation (DFG) under the project *SO 320/4-2*

the origin $(x, y; \cdot) = (\mathbf{0}; \cdot)$ of a local coordinate system to $f_p = n\ a\cos\phi$. In case of image analysis lines, edges, junctions and corners can be modeled in this way. The signal processing task is now to determine the local amplitude $a = a_s$, the local orientation $\theta_\nu = \theta_{s,\nu}$ and the local phase $\phi = \phi_s$ for a certain scale space parameter s. This problem has been already solved for one-dimensional signals by the classical analytic signal [8] by means of the Hilbert transform [9] and for intrinsically one-dimensional [19] signals (i.e. $n = 1$ in Equation (1)) by the 2D monogenic signal [4] by means of the generalized first order Hilbert transform. This paper shows that 2D signal processing can be regarded as an inverse problem [16] where higher order generalized 2D Hilbert transforms are applied to the original signal f, here with the signal model in Equation (1) restricted to $n < 3$ in Equation (1). 2D signals in scale space are classified into local regions $N \subseteq \Omega$ of different intrinsic dimensions [19] (which correspond to their codimension). The intrinsic dimension expresses the number of degrees of freedom necessary to describe local structure. Constant signals are of intrinsic dimension zero (i0D), straight lines and edges are of intrinsic dimension one (i1D) and all other possible patterns such as corners and junctions are of intrinsic dimension two (i2D) (see Figure 1)

$$\text{i0D} = \{f : f(z_i) = f(z_j)\ \forall z_i, z_j \in N\} \tag{3}$$

$$\text{i1D} = \{f : f(z) = g(\langle z, \bar{o}\rangle)\ \forall z \in N\} \setminus \text{i0D} \tag{4}$$

$$\text{i2D} = \left(L^2(\mathbb{R}^2) \cap L^1(\mathbb{R}^2)\right) \setminus (\text{i0D} \cup \text{i1D}) \tag{5}$$

with $g \in L^2(\mathbb{R}) \cap L^1(\mathbb{R})$ and $\bar{o} = [\cos\theta, \sin\theta]^T$. In general i2D signals can only be modeled by an infinite number of superimposed i1D signals. Therefore, it is essential to assume a certain signal model or a set of certain models for exact i2D signal analysis. Furthermore, the intrinsic dimension depends also on the scale space parameter s at which the signal will be considered locally.

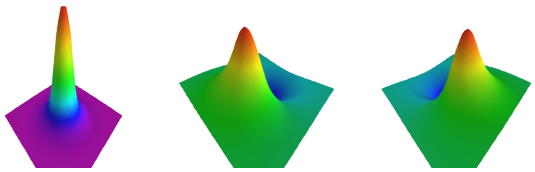

Figure 2. From left to right: Poisson convolution kernel $p(z; s)$ and conjugate Poisson convolution kernels $q_x^{(1)}(z; s)$ and $q_y^{(1)}(z; s)$ in spatial domain for a certain scale space parameter $s > 0$.

3. Related work: the monogenic signal

Related work is the recently introduced monogenic signal [4] which can be regarded as the Hilbert transform based analogue to the derivative based gradient. The first order generalized Hilbert transform kernel [1] can be expressed in

[1]The generalized first order 2D Hilbert (or Riesz) transform convolution kernel reads $h^{(1)}(z) = \frac{1}{2\pi\|z\|^3}\,[x, y]^T$

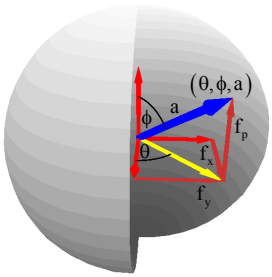

Figure 3. Geometric illustration and interpretation of the 2D monogenic signal vector $[f_p, f_x, f_y]^T$ features as spherical coordinates (θ, ϕ, a) in 3D Euclidean space. This descriptive geometric interpretation will be generalized and extended to the projective space in this work.

Poisson scale space by

$$q^{(1)}(z; s) = (p * h^{(1)})(z; s) = \frac{1}{2\pi\,(s^2 + \|z\|^2)^{3/2}} \begin{bmatrix} x \\ y \end{bmatrix} \tag{6}$$

The 2D monogenic signal can be defined as a vector valued signal representation $[f_p, f_x, f_y]^T$ where the first order Hilbert transformed signal $[f_x, f_y]^T = (q^{(1)} * f)(\mathbf{0}; s)$ can be expressed in Radon space [16] (proof: [16]) by the important relation

$$\begin{bmatrix} f_x \\ f_y \end{bmatrix} = \mathcal{R}^{-1}\left\{ \begin{bmatrix} \cos\theta \\ \sin\theta \end{bmatrix} h(t) * f_r(t; \theta; s) \right\} (\mathbf{0}; s) \tag{7}$$

with the 2D Radon transformed signal (see Figure 4)

$$f_r(t, \theta; s) = \int_{z \in \mathbb{R}^2} \mathcal{P}\{f\}(z; s)\,\delta\left(\langle z, \bar{o}\rangle - t\right)\, dz \tag{8}$$

with $z = (x, y)$, $\bar{o} = [\cos\theta, \sin\theta]^T$, $\theta \in [0, \pi)$ as the orientation, $t \in \mathbb{R}$ as the minimal distance of the line to the origin $(\mathbf{0}) \in \mathbb{R}^2$ of the local coordinate system and δ as the Dirac delta distribution. The inverse 2D Radon transform exists and reads

$$\begin{aligned} \mathcal{R}^{-1}\{f_r\}(\mathbf{0}) &= \frac{1}{2\pi^2} \int_{\theta \in [0,\pi)} \text{P.V.} \int_{t \in \mathbb{R}} \frac{\frac{\partial}{\partial t} f_r(t, \theta; s)}{\langle z, \bar{o}\rangle - t} dt\, d\theta \\ &= -\frac{1}{2\pi^2} \sum_{\nu=1}^{n} \text{P.V.} \int_{t \in \mathbb{R}} \frac{\frac{\partial}{\partial t} f_r(t, \theta_\nu; s)}{t} dt \end{aligned}$$

with P.V. as the Cauchy principal value and the classical 1D Hilbert transform kernel [2] $h(t) = \frac{1}{\pi t}$. The main advantage of this expression in 2D Radon space is the resulting system of equations [16]

$$\begin{bmatrix} f_x \\ f_y \end{bmatrix} = \sum_{\nu=1}^{n} \begin{bmatrix} \cos\theta_\nu \\ \sin\theta_\nu \end{bmatrix} a \sin\phi \tag{9}$$

[2]Both the classical 1D Hilbert transform as well as all generalized Hilbert transforms intrinsically always remain in one-dimension, i.e. in this work the function $f(t) = a\cos(t)$ will be considered and its Hilbert transform $(f * h)(t) = a\sin(t)$ with the property $(f * h * h)(t) = -f(t)$.

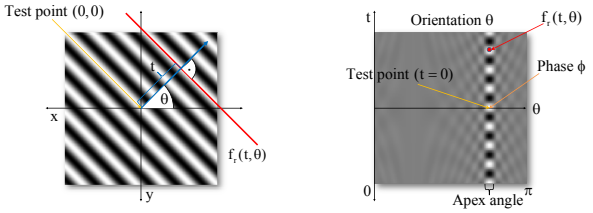

Figure 4. Left figure: i1D signal f_p in spatial domain with orientation θ_m and local phase $\phi = 0$ at the origin $(\mathbf{0}) \in \mathbb{R}^2$ of the applied local coordinate system. Right figure: i1D signal f_p in Radon space. Each point in Radon space represents the integral in spatial domain on a line which is uniquely defined by the minimal distance $t \in \mathbb{R}$ to the origin and the orientation $\theta \in [0, \pi)$. The Radon transform of the Poisson filtered signal will be abbreviated by $f_r(t, \theta) = \mathcal{R}\{\mathcal{P}\{f\}\}(t, \theta)$.

with the explicit formulation of the signal features. This system of equations has to be solved for the unknown signal model features. In case of i1D signals (i.e. $n = 1$ in Equation (1)) this system of equations degrades to

$$\begin{bmatrix} f_p \\ f_x \\ f_y \end{bmatrix} = a \begin{bmatrix} \cos\phi \\ \sin\phi\cos\theta \\ \sin\phi\sin\theta \end{bmatrix} \tag{10}$$

which can be now solved for the 3D spherical coordinates (see Figure 3)

$$\theta = \arctan\frac{f_y}{f_x} \tag{11}$$

$$\phi = \operatorname{atan2}\left(\sqrt{f_x^2 + f_y^2}, f_p\right) \tag{12}$$

$$a = \sqrt{f_p^2 + f_x^2 + f_y^2}\,. \tag{13}$$

The phase vector $\Phi_{2D}(z)$ of the monogenic signal is defined by

$$\Phi_{2D}(z) = \begin{bmatrix} \Phi_x \\ \Phi_y \end{bmatrix}(z) = \phi_s \begin{bmatrix} \cos\theta_s \\ \sin\theta_s \end{bmatrix} \tag{14}$$

Since the 2D monogenic signal is strictly limited to the class of i1D signals, the aim of this work is to find and solve an appropriate geometrical interpretation for i1D and i2D signals in one framework.

4. Second order Hilbert transforms

In case of i2D signals (i.e. $n > 1$ in Equation (1)) the resulting system of equations delivered solely by the first order generalized Hilbert transform in 2D Radon space is not sufficient for the solution of all signal features. Therefore, we have to make use of the higher order generalized Hilbert transforms, such as the second order Hilbert transform kernels [16] (see Figure 5)

$$q^{(2)}(z; s) = \frac{3s\|z\|^2 + 2s^3 - 2(\|z\|^2 + s^2)^{3/2}}{2\pi\|z\|^4(\|z\|^2 + s^2)^{3/2}} \begin{bmatrix} x^2 \\ xy \\ y^2 \end{bmatrix} \tag{15}$$

with $z = (x, y)$ and $q^{(2)} = q^{(1)} * h^{(1)}$ to determine the second order Hilbert transformed signal $[f_{xx}, f_{xy}, f_{yy}]^T = (q^{(2)} * f)(\mathbf{0}; s)$ which can be also expressed by

$$\begin{bmatrix} f_{xx} \\ f_{xy} \\ f_{yy} \end{bmatrix} = -\mathcal{R}^{-1}\left\{ \begin{bmatrix} \cos^2\theta \\ \sin\theta\cos\theta \\ \sin^2\theta \end{bmatrix} f_r(t, \theta; s) \right\}(\mathbf{0}; s) \tag{16}$$

in 2D Radon space. Analogously to the first order Hilbert transform the following additional system of equations results of the second order Hilbert transformed signal

$$\begin{bmatrix} f_{xx} \\ f_{xy} \\ f_{yy} \end{bmatrix} = \sum_{\nu=1}^{n} \begin{bmatrix} \cos^2\theta_\nu \\ \frac{1}{2}\sin(2\theta_\nu) \\ \sin^2\theta_\nu \end{bmatrix} a\cos\phi\,. \tag{17}$$

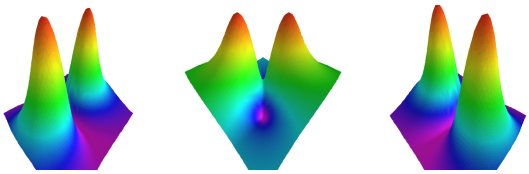

Figure 5. From left to right: second order Hilbert transform convolution kernels in spatial domain $q_{xx}^{(2)}(x, y; s)$, $q_{xy}^{(2)}(x, y; s)$ and $q_{yy}^{(2)}(x, y; s)$ for a certain scale space parameter $s > 0$.

5. The 2D analytic signal

By the first and second order generalized Hilbert transforms the monogenic signal can be now generalized to the novel 2D analytic signal. Analogous to the Hesse matrix (known from surface theory) the second order partial derivatives will be substituted by the second order Hilbert transformed signals in the corresponding directions. This matrix valued signal representation

$$T^e = \begin{bmatrix} f_{xx} & f_{xy} \\ f_{xy} & f_{yy} \end{bmatrix} \in M(2, \mathbb{R}) \tag{18}$$

can be mapped to a vector valued signal representation by the isomorphism [16]

$$([f_p, f_x, f_y]^T, T^e) \cong [f_p, f_x, f_y, f_s, f_+, f_{+-}]^T \tag{19}$$

with $f_s = \frac{1}{2}[f_{xx} + f_{yy}] = \frac{1}{2}f_p$, $f_+ = f_{xy}$ and $f_{+-} = \frac{1}{2}[f_{xx} - f_{yy}]$ (see Figure 6). This isomorphism delivers the convolution kernels being the key for geometrical signal interpretation in projective space.

5.1. Signal representation in projective space

The local features which determine the signal in scale space will be separated in geometrical features and structural features. The geometrical features are the mean orientation and the rotationally invariant apex angle. The mean orientation

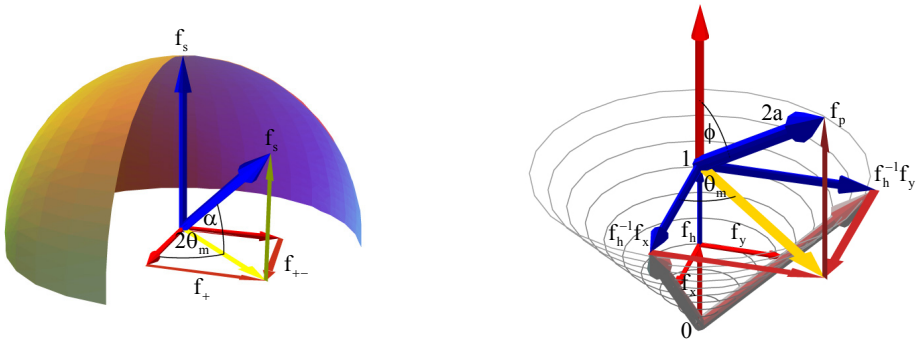

Figure 7. Left figure: geometric interpretation of the mean orientation θ_m and the apex angle α. The 2D analytic signal strictly separates the structural and the geometrical information delivered by the first and the second order Hilbert transform respectively. Right figure: geometric interpretation of phase ϕ, amplitude a and main orientation θ_m in projective space of i1D and i2D signals in one unified framework.

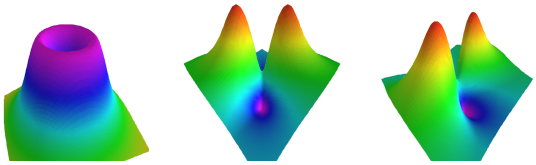

Figure 6. From left to right: convolution kernels which deliver f_s, f_+ and f_{+-} for a certain scale space parameter $s > 0$ in spatial domain.

[3] can be determined by

$$\theta_m = \frac{\theta_1 + \theta_2}{2} = \frac{1}{2} \arctan \frac{f_+}{f_{+-}} \ . \tag{20}$$

The apex angle $\alpha = \theta_1 - \theta_2$ (also known as opening angle) can be determined by

$$\alpha = \arccos \frac{\sqrt{f_+^2 + f_{+-}^2}}{\|f_s\|} = \arctan \frac{\sqrt{f_s^2 - \left[f_+^2 + f_{+-}^2\right]}}{\sqrt{f_+^2 + f_{+-}^2}} \tag{21}$$

which delivers in combination with θ_m the individual orientations θ_1 and θ_2. The apex angle [4] is a very important rotationally invariant local feature since it is zero iff the underlying structure is of intrinsic dimension one (see Figure 9). The geometric interpretation of the mean orientation and the apex angle results from the signal f_s which is embedded in 3D space as a vector $[0, 0, f_s]^T \in \mathbb{R}^3$. This 3D vector will be rotated by the Euler angles $(\alpha, 2\theta_m) \in \left[0, \frac{\pi}{2}\right] \times [0, 2\pi]$ (see Figure 7). By means of the apex angle α, a so called homogeneous signal component f_h of the signal f_p in 3D projective space [14] can be now introduced by

$$f_h = \sqrt{\frac{1 + \cos\alpha}{2}} \in [0, 1] \ . \tag{22}$$

[3] In contrast to the monogenic signal the mean orientation [15] can be evaluated also at phase positions $\phi = k\pi$ for all $k \in \mathbb{Z}$ where the orientation of the monogenic signal $\frac{1}{2}\left[\theta_1 + \theta_2\right] = \arctan \frac{f_y}{f_x}$ is not defined.

[4] Note that the apex angle of phase based image analysis corresponds to the shape feature of the orthogonal version of the second order derivatives [3] although they are not equal.

In the following a natural relation of the vector valued 2D analytic signal representation and the projective space will be shown. By means of the homogeneous signal component the model based signal features can be now determined. The local main orientation of the signal can be determined by

$$\theta_m = \arctan \frac{f_h^{-1} f_y}{f_h^{-1} f_x} \tag{23}$$

which corresponds to Equation (11). The structural signal features are the local phase and the local amplitude. The phase of i1D and i2D signals can be evaluated by

$$\phi = \operatorname{atan2}\left(\sqrt{\left[f_h^{-1} f_x\right]^2 + \left[f_h^{-1} f_y\right]^2}, f_p\right) \tag{24}$$

which is the generalization of Equation (12) for i1D and i2D signals in one unified framework. The local amplitude for i1D and i2D signals can be determined by

$$a = \frac{1}{2}\sqrt{f_p^2 + \left[f_h^{-1} f_x\right]^2 + \left[f_h^{-1} f_y\right]^2} \tag{25}$$

which is the generalization of Equation (13) for i1D and i2D signals in one unified framework. The phase and the amplitude can be determined by the first order Hilbert transform and the geometric information given by the apex angle and the main orientation will be delivered by the higher order Hilbert transform. In the case of pure i1D signals the apex angle is zero, i.e. $f_h = 1$. In this case the formulas of the phase and amplitude reduce to those known from the monogenic signal. The advantage of this approach is that it can automatically distinguish between i1D and i2D signals and it can be applied to all kinds of local intrinsic dimension without any previous knowledge about the original signal. In the case of 2D image signals, this approach is designed for an isotropic analysis of lines, edges, corners and junctions in one framework. The important generalization from i1D signal analysis to true 2D signal analysis is, that in contrast to the 2D monogenic signal, here the 2D conjugate Poisson components $[f_x, f_y]^T$ are in a natural way located

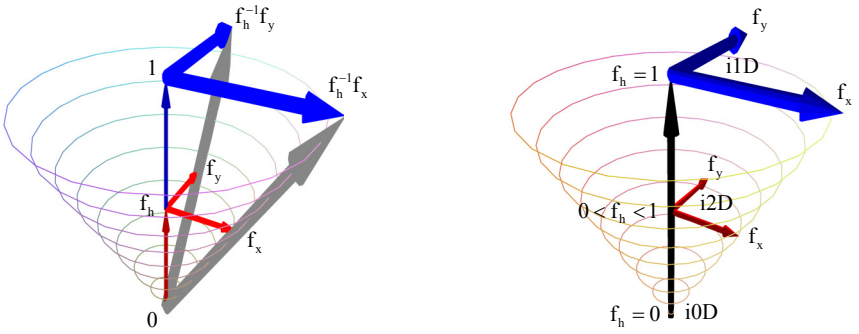

Figure 8. Left figure: the underlying 2D space is spanned by the conjugate signal components f_x and f_y and the additional coordinate of the 3D projective space is given by the homogeneous signal component f_h. Right figure: illustration of all intrinsic dimensions in one continuous space. The i0D signals are on a point of singularity, the i1D signals can be represented by a 2D plane and the i2D signals exist in a 3D volume.

in the higher dimensional 3D projective space $[f_x, f_y, f_h]^T$ with f_h as the additional homogeneous signal component (see Figure 8). Signal analysis naturally reduces now to the normalization of the homogeneous component to 1 (see Figure 8). This can be easily done by multiplying the conjugate Poisson signal components f_x and f_y by f_h^{-1}. In other words: The 2D space spanned by the signal components f_x and f_y is extended by the homogeneous signal component f_h.

5.2. Proof outline

Due to the previous results of the first and second order generalized Hilbert transform expressed in Radon space (see Figure 10) the proofs can now be done by trigonometric calculations using the known local signal components

$$\begin{bmatrix} f_p \\ f_x \\ f_y \\ f_s \\ f_+ \\ f_{+-} \end{bmatrix} = a \begin{bmatrix} 2\cos\phi \\ \sin\phi\,[\cos\theta_1 + \cos\theta_2] \\ \sin\phi\,[\sin\theta_1 + \sin\theta_2] \\ \cos\phi \\ \cos\phi\frac{1}{2}\,[\sin(2\theta_1) + \sin(2\theta_2)] \\ \cos\phi\frac{1}{2}\,[\cos(2\theta_1) + \cos(2\theta_2)] \end{bmatrix} \tag{26}$$

which results from the signal intelligence in Radon space. Note that the relation to the Radon transform is required solely for interpretation and theoretical results. Neither the Radon transform nor its inverse are ever applied to the signal in practice. Instead, the generalized Hilbert transformed signal components will be determined by a 2D convolution with the generalized Hilbert transform kernels in spatial domain.

6. Implementation of the 2D analytic signal

The 2D analytic signal can be easily integrated into any computer vision software package by using the following C++ implementation. Each DC-free signal `double f(double x,double y)` can be locally analyzed in scale space at every position $(c_x, c_y) \in \mathbb{R}^2$ by applying a difference of Poisson (DoP) [5] bandpass filter to the original signal with the fine scale space parameter s_f and the coarse scale space parameter s_c.

```
void AnalyticSignal2D(
     double cx,double cy,
     double& Orientation,double& Apexangle,
     double& Amplitude,double& Phase,
     double s_c=2,double s_f=1.9,double m=3)
{
  double f_p =0,f_x =0,f_y =0;
  double f_xx=0,f_xy=0,f_yy=0;
  for (double x = -m;x <= m;x++)
  for (double y = -m;y <= m;y++)
  {
    double t  = f(x+cx,y+cy);
    double pf = t* Kernel1(x,y,s_f);
    double pc = t* Kernel1(x,y,s_c);
    double k  = t*(Kernel2(x,y,s_f)-
                   Kernel2(x,y,s_c));
    f_p  += s_f*pf - s_c*pc;
    f_x  += x   * (pf-pc);
    f_y  += y   * (pf-pc);
    f_xx += x*x * k;
    f_yy += y*y * k;
    f_xy += x*y * k;
  }
  double f_pm = 0.5*(f_xx-f_yy);
  double f_s  = 0.5* f_p;
  double e = sqrt(pow(f_pm,2)+
             pow(f_xy,2))/fabs(f_s);
  double l = pow(f_x,2)+pow(f_y,2);
  double q = l*2/(1+e);
  Phase       =atan2(sqrt(q),f_p);
  Orientation=0.5*atan2(f_xy,f_pm);
  Amplitude  =0.5*sqrt(pow(f_p,2)+q);
  ApexAngle=atan2(sqrt(pow(f_s,2)-
            pow(f_xy,2)-pow(f_pm,2)),
            sqrt(pow(f_xy,2)+pow(f_pm,2)));
}
```

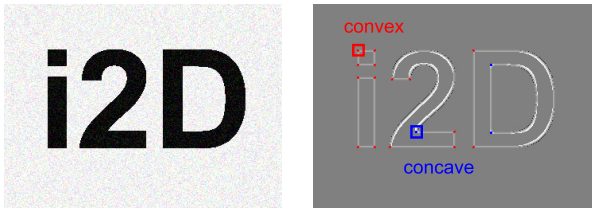

Figure 9. From left to right: original image signal and its local apex angle. The apex angle can not only separate corners/junctions from edges/lines but also distinguish between convex and concave corners.

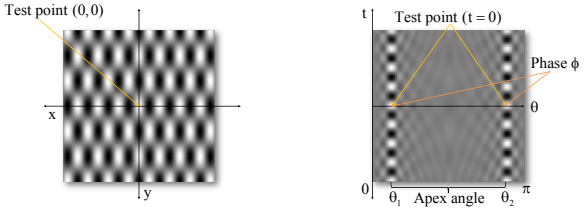

Figure 10. Left figure: The i2D checkerboard signal in spatial domain with orientations θ_1, θ_2 and local phase $\phi = 0$ at the test point $(x, y) = (\mathbf{0})$ at the origin of the local coordinate system. Right figure: The i2D signal is separated into two independent i1D signals with different orientations and same phase at $t = 0$ in 2D Radon space.

The first order generalized 2D Hilbert convolution kernels will be calculated by

```
double Kernel1(double x,double y,double s)
{
  double S=pow(s,2),K=pow(x,2)+pow(y,2);
  return 1/(2*M_PI*pow(S + K,1.5));
}
```

and the second order generalized 2D Hilbert convolution kernels in spatial domain with scale space parameter s will be determined by

```
double Kernel2(double x,double y,double s)
{
  double S=pow(s,2),K=pow(x,2)+pow(y,2);
  double d=pow(K,2)*pow(S+K,1.5)*2*M_PI;
  return -(s*(2*S+3*K)-2*pow(S+K,1.5))/d;
}
```

The orientation, apex angle, amplitude and phase are being calculated as distinctive local features of the signal for a given convolution mask size m. The time complexity of this algorithm is in $O(m)$ with m as the total convolution mask size. This time complexity can be reduced by calculation in Fourier domain. The disadvantage of the calculation in Fourier domain is the restriction to a global signal analysis with one fixed scale space parameter for the entire image. By convolution in spatial domain for each position $(x, y; s) \in \mathbb{R}^2 \times \mathbb{R}_+$ an individual scale space parameter can be chosen to enable adaption to the local structural and geometrical signal information. Note that in case of arbitrary signals only DC-free convolution kernels can be used. This can be achieved by removing the mean value of the convolution kernels after precalculating them and before applying them to signal analysis.

7. Experimental results and comparison

In the following the 2D analytic signal and the 2D monogenic signal [4] will be applied to synthetic signals for comparison and qualitatively results. Figure (11) illustrates the experimental results with known ground truth data (amplitude, phase, and orientation) of the 2D monogenic signal. The estimated features are plotted with fixed orientation and fixed amplitude against varying phase $0 \leq \phi \leq 180°$ and varying apex angle $0 \leq \alpha \leq 90°$. The left plot in Figure (11) depicts a subset of the test signals. In the following the experimental results of the 2D monogenic signal are being discussed from left to right. The orientation can be determined exactly except for the phases $\phi = 0°$ and $\phi = 180°$. The amplitude is disturbed even in case of i1D signals, i.e. at zero apex angle, and should be globally constant like the results shown in Figure (12). The phase errors increase with increasing apex angle. In the ideal case the result should look like the plane in Figure (12). These results show that in contrast to the 2D analytic signal, the amplitude and phase of the 2D monogenic signal produce significant errors. *It is very important to mention that the novel 2D analytic signal performs also in case of finite i1D signals better than the 2D monogenic signal although in theory for zero apex angle both signals are the same.* But for finite signals the local apex angle is never totally zero since the i1D signal slice in 2D Radon space is always broadened, see Figure (4). This broadness will be detected by the 2D analytic signal automatically resulting in an apex angle greater than zero in contrast to the 2D monogenic signal which ignores this feature by assuming a zero apex angle.

Analogously to the results of the 2D monogenic signal the experimental results of the 2D analytic signal are illustrated in Figure (12) with same experimental settings. Left plot: estimated apex angle for varying phase and varying apex angle. The apex angle can be determined exactly. Second plot from left to right: estimated orientation for varying phase and varying apex angle but fixed signal orientation and fixed signal amplitude. The orientation can be determined exactly except for the phase singularity $\phi = 180°$. Third plot from left to right: estimated amplitude for varying phase and varying apex angle but fixed signal amplitude. The amplitude can be determined exactly as a constant value. Right plot: estimated phase for varying phase and varying apex angle. The phase can be determined exactly by the 2D analytic signal.

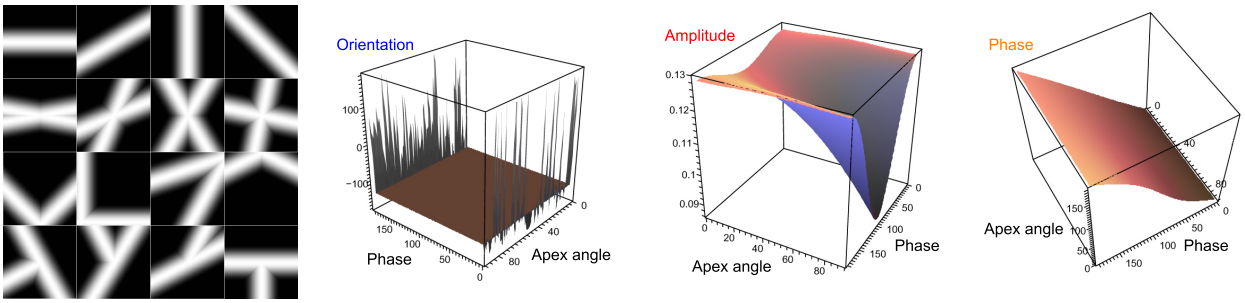

Figure 11. Results of the monogenic signal. First figure from top to bottom row: test signals consisting of lines/edges, x-junctions, corners and t/y junctions. Second to last figure: local orientation, amplitude and phase results. Convolution mask size in spatial domain: 7×7 pixels. Coarse scale space parameter: $s_c = 0.2$, and fine scale space parameter: $s_f = 0.1$.

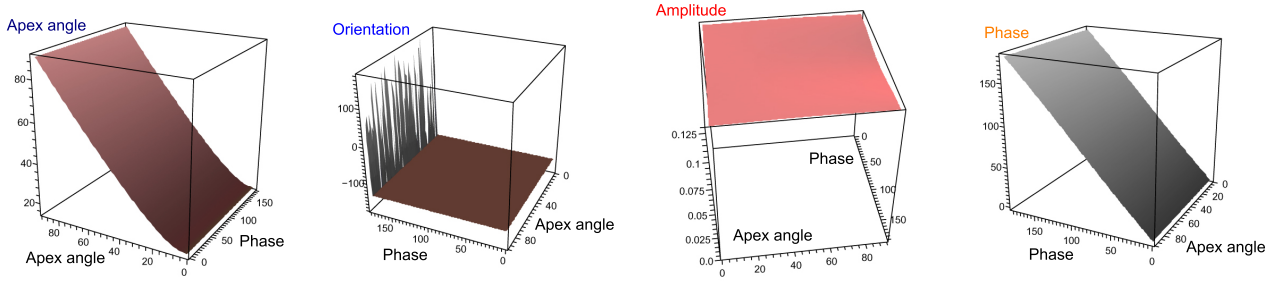

Figure 12. Experimental results of the 2D analytic signal. From left to right: local apex angle, orientation, amplitude and phase results. Convolution mask size in spatial domain: 7×7 pixels. Coarse scale space parameter: $s_c = 0.2$, and fine scale space parameter: $s_f = 0.1$.

8. Application: dense optical flow

The 2D analytic signal is an ideal substitute for the partial Hilbert transform [9], the 2D monogenic signal [4] and for all applications which make use of derivatives (e.g. the Laplacian) in detection of local features, e.g. texture analysis, layer separation and vessel detection in medical image processing. In optical flow applications the intensity or the mostly used gradient constancy constraint can be easily replaced by the novel 2D analytic signal phase vector $\Phi_{3D}(z) \in \mathbb{R}^3$

$$\Phi_{3D}(z) = \begin{bmatrix} \Phi_x \\ \Phi_y \\ \Phi_z \end{bmatrix}(z) = \phi_s \begin{bmatrix} \cos\theta_s \\ \sin\theta_s \cos\alpha_s \\ \sin\theta_s \sin\alpha_s \end{bmatrix} \tag{27}$$

consisting of the rotationally invariant local apex angle α_s, the local main orientation θ_s and the local i1D/i2D phase ϕ_s with scale space parameter s to minimize the resulting nonlinear energy functional [1]

$$E(w) = \int_{z\in\Omega} \underbrace{\lambda\Psi(\|\nabla u(z)\|^2 + \|\nabla v(z)\|^2)}_{\text{Smoothness term}} \tag{28}$$

$$+ \underbrace{\sum_{\iota\in\{x,y,z\}} \Psi(\|\Phi_\iota(z+w(z)) - \Phi_\iota(z)\|^2)\; dz}_{\text{Data term}} \tag{29}$$

with $z = (x, y)$, the unknown optical flow $w(z) = [u(z), v(z)]$, $\lambda > 0$ as a weighting factor of the smoothness term and $\Psi(s^2) = \sqrt{s^2 + \epsilon^2}$ as a penalizing function

Scenario	[13]	Φ_{3D}	Φ_{2D}	∇
Cloudy Yosemite	2.44°	1.77°	2.11°	2.39°
Yosemite	1.64°	0.91°	1.33°	1.60°
Street	4.93°	4.10°	4.55°	4.87°
Marble	4.74°	3.98°	4.47°	4.81°

Table 1. Comparison of the average angular error (AAE) [13] of the classical gradient ∇, the phase vector Φ_{2D} of the 2D monogenic signal and the novel phase vector Φ_{3D} of the 2D analytic signal used as the constancy constraint for dense optical flow estimation.

for a small constant ϵ. Note that the involved scale space approach automatically provides a multi-resolution or fine-to-coarse warping strategy. Results of the gradient [13] versus the phase vector are presented in Table (1). The advantage of the phase vector is the invariance against global and local illumination change and the robustness against noise (see Figure 13).

9. Conclusion

In this work a generalization of the classical analytic signal to the isotropic 2D analytic signal has been presented. Both i1D and i2D image signals such as edges, lines, corners and junctions can be rotationally invariant analyzed in one unified framework in scale space without any steering

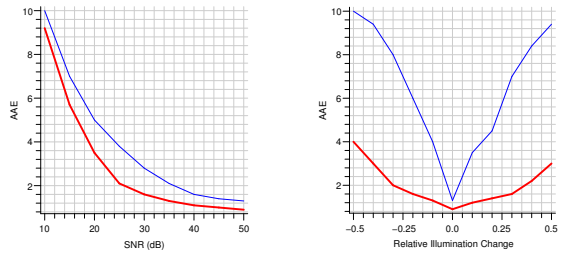

Figure 13. Experimental results of the average angular error (AAE) [13] in optical flow estimation applications. Comparison of classical derivative based (thin blue line) constancy constraints and the phase vector (thick red line) delivered by the 2D analytic signal. Left figure shows that the phase vector is much more robust against additive Gaussian noise. Right figure: Since the 2D analytic signal delivers a split of identity where the amplitude information is orthogonal to the phase information, the phase vector is invariant against global and local illumination changes compared to derivatives.

[11]. Our approach naturally degenerates to the 2D monogenic signal for the case of i1D signals. Distinctive local signal features such as amplitude, phase, apex angle and orientation span an orthogonal feature space (split of identity). The 2D analytic signal can be easily implemented into existing computer vision applications by locally adaptive 2D convolution in spatial domain. It has been shown that the 2D analytic signal performs better than the 2D monogenic signal even for i1D signals. We presented a further step in the evolution process of the complex valued analytic signal by D. Gabor to the 2D analytic signal which maps a real valued signal to a vector valued signal in homogeneous conformal space. This can be geometrically interpreted in an intuitive and descriptive way in the projective subspace of the conformal space. One very important philosophical result is that signal analysis of i1D and i2D signals in one unified framework corresponds to the extension of the so far used Euclidean space to the higher dimensional projective space. Our future work contains the extension of the 2D analytic signal to a tensor valued signal by using also the third order Hilbert transform.

References

[1] T. Brox, A. Bruhn, N. Papenberg, and J. Weickert. High accuracy optical flow estimation based on a theory for warping. In *ECCV*, volume 4 of *LNCS 3024*, pages 25–36. Spinger, 2004.

[2] G. Carneiro and A. D. Jepson. Phase-based local features. In *7th European Conference on Computer Vision-Part I*, volume 2350 of *LNCS*, pages 282–296. Springer-Verlag, Berlin, Heidelberg, New York, 2002.

[3] P. E. Danielsson, Q. Lin, and Q. Z. Ye. Efficient detection of second-degree variations in 2D and 3D images. *Journal of Visual Communication and Image Representation*, 12(3):255–305, 2001.

[4] M. Felsberg and G. Sommer. The monogenic signal. *IEEE Transactions on Signal Processing*, 49(12):3136–3144, 2001.

[5] M. Felsberg and G. Sommer. The monogenic scale-space: A unifying approach to phase-based image processing in scale-space. *Journal of Mathematical Imaging and Vision*, 21:5–26, 2004.

[6] D. J. Fleet and A. D. Jepson. Stability of phase information. *IEEE Transactions on Pattern Analysis and Machine Intelligence*, 15(12):1253–1268, 1993.

[7] D. J. Fleet, A. D. Jepson, and M. R. M. Jenkin. Phase-based disparity measurement. *CVGIP: Image Understanding*, 53, 1991.

[8] D. Gabor. Theory of communication. *Journal IEE, London*, 93(26):429–457, 1946.

[9] S. L. Hahn. *Hilbert Transforms in Signal Processing*. Artech House Inc, Boston, London, 1996.

[10] T. Huang, J. Burnett, and A. Deczky. The importance of phase in image processing filters. *IEEE Trans. on Acoustics, Speech and Signal Processing*, 23(6):529–542, 1975.

[11] M. Jacob and M. Unser. Design of steerable filters for feature detection using Canny-like criteria. *IEEE Transactions on Pattern Analysis and Machine Intelligence*, 26(8):1007–1019, 2004.

[12] A. V. Oppenheim and J. S. Lim. The importance of phase in signals. *Proceedings of the IEEE*, 69(5):529–541, 1981.

[13] N. Papenberg, A. Bruhn, T. Brox, S. Didas, and J. Weickert. Highly accurate optic flow computation with theoretically justified warping. *International Journal of Computer Vision*, 67(2):141–158, 2006.

[14] C. Perwass. *Geometric Algebra with Applications in Engineering*, volume 4 of *Geometry and Computing*. Springer-Verlag, Berlin, Heidelberg, 2009.

[15] B. Rieger and L. J. van Vliet. Representing orientation in n-dimensional spaces. In *CAIP*, volume 2756 of *LNCS*, pages 17–24. Springer-Verlag, Berlin, Heidelberg, New York, 2003.

[16] L. Wietzke and G. Sommer. The 2D analytic signal. Technical Report 0802, Kiel University, Department of Computer Science, 2008.

[17] Z. Xiaoxun and J. Yunde. Local steerable phase (lsp) feature for face representation and recognition. In *CVPR '06: Proceedings of the 2006 IEEE Computer Society Conference on Computer Vision and Pattern Recognition*, pages 1363–1368. IEEE Computer Society, 2006.

[18] D. Zang, L. Wietzke, C. Schmaltz, and G. Sommer. Dense optical flow estimation from the monogenic curvature tensor. In *Scale Space and Variational Methods*, volume 4485 of *LNCS*, pages 239–250. Springer-Verlag, Berlin, Heidelberg, New York, 2007.

[19] C. Zetzsche and E. Barth. Fundamental limits of linear filters in the visual processing of two-dimensional signals. *Vision Research*, 30:1111–1117, 1990.